Energy Technology
Generation, Conversion, Storage, Distribution
www.entechnol.de

Enhanced Silicon Photovoltaic Efficiency by Solar Light Spectral Modulation via Photonically Tuned Porphyrin–Iron Oxide Hybrid Thin Films

*Mengyao Lyu, Jou Lin, Yuxin Wang, Ovais Aulakh, Nathan Ceja, Mary Sheryl Ramesh, Elisabeth Salazar, John Krupczak, and Donglu Shi**

The temperature dependency of photovoltaic power conversion efficiency (PCE) has been a key challenge to solar applications due to intrinsic processes. Herein, an alternative strategy is developed by modulating the solar light spectrum with a series of photonic hybrids. Transparent thin films are synthesized with the solutions of porphyrin compounds and iron oxides which exhibit strong absorptions in the UV and IR regions. These spectral modulating thin films are photonically tuned via compositional optimization to absorb photons near 400 nm and above 1127 nm from solar spectrum to reduce thermalization and sub-bandgap absorption. These spectral modulators are applied in a particular configuration above a commercial silicon panel to partially filter the simulated solar light. The PCE of the silicon panel suffers a significant decrease due to temperature increase from 22.9 to 92.9 °C after 60 min solar irradiation, resulting in a PCE decrease from 25.1% to 16.3%. With the transparent spectral modulators, upon solar irradiation for 60 min, the maximum PCE has maintained at 20.5%. The mechanisms of PCE enhancement are identified based on reduced thermalization and sub-bandgap absorption.

1. Introduction

To achieve environmentally sustainable systems that are energy neutral, zero emission, and climate positive, utilization of solar energy has been the main approach to produce clean energy for many technical, environmental, and ecological advantages.[1–5] Although photovoltaic (PV) solar panels have been most popular and widely employed for a variety of applications,[6–9] the power conversion efficiencies (PCEs) of the commercial PV panels have been limited. The conventional silicon solar panels have so far achieved efficiencies on the order of 20%−30%.[10–15] A variety of solar panel materials have also been developed including amorphous silicon, copper indium gallium selenide, and cadmium telluride.[16] Recently, the research on the perovskite solar cells (PSCs) has become increasingly ubiquitous for their attractive properties and manufacturing advantages as compared to some of the conventional PV solar panels. However, the PCEs of PSCs remain comparable (23.7%) to those of the silicon-based PVs.[17]

In retrospect, the improvement in PCE of all solar panels has been incremental in the last 30 years, only a few degrees of increase, due to intrinsic limitations. The key barrier in PCE enhancement is described by the so-called Shockley–Queisser limit (SQ limit).[18] The model basically considers all-aspects of intrinsic limitations, majorly from blackbody radiation, recombination, and spectrum losses. The SQ model assumes blackbody radiation from solar panel at room temperature (300 K) accounting about 7% of energy falling on the panel. As the energy lost in a panel is converted to heat, the panel temperature increases to reach an equilibrium as high as 360 K, resulting in a lower PCE than that at 300 K. Recombination is an intrinsic behavior that takes place via a state in the bandgap, associated with a crystal defect.

Spectral losses originate from distribution of incoming photon energy in relation to the bandgap (E_g). For E_g of silicon (1.1 eV), those photons with lower energies, denoted as the sub-bandgap absorption, will not contribute to the short-circuit current (I_{SC}).[19] Within the solar spectrum, about 19% photons have energies less than 1.1 eV, which is about 33% of the incident sun light. However, for photons with energies much greater than E_g, thermalization sets in and contributes to spectral losses.[20] Within picoseconds, electrons are excited to occupy higher levels of the conduction band, and then quickly relaxed to near the conduction band edge. In this process, thermal energy is dissipated as a major loss mechanism of thermalization.

M. Lyu, J. Lin, Y. Wang, D. Shi
The Materials Science and Engineering Program, Department of Mechanical and Materials Engineering, College of Engineering and Applied Science
University of Cincinnati
Cincinnati, OH 45221, USA
E-mail: shid@ucmail.uc.edu

O. Aulakh, N. Ceja, M. S. Ramesh, E. Salazar, J. Krupczak
Department of Engineering
Hope College
Holland, MI 49423, USA

The ORCID identification number(s) for the author(s) of this article can be found under https://doi.org/10.1002/ente.202300144.

DOI: 10.1002/ente.202300144

SQ has considered these intrinsic processes and concluded a maximum limit of 33.7% of PCE for single p–n junction silicon with a bandgap of 1.4 eV (using an AM1.5 solar spectrum).[18] Ever since then, no solar panels have broken this barrier experimentally, therefore setting an upper limit for all current semiconductor PV panels. Among all loss mechanisms, thermalization originating from high-energy photons near UV is one of the major losses accounting for a maximum up to 49% of the incident energy.[21,22] IR heating due to sub-bandgap absorption is another important factor that limits PCE especially for prolonged solar irradiation during daytime.

In this study, we designed a series of transparent nanohybrid thin films to spectrally modulate the solar light in the designated frequency regions for suppressing both thermalization and sub-bandgap absorption. The concept of spectral modulator is schematically illustrated in **Figure 1**. As shown in this figure, a transparent spectral modulator (TSM) is placed under the solar simulator so that the light passes through it, shining on a commercial silicon PV panel (54 mm × 54 mm 2 V 130 mA Micro Solar Panels). These TSMs are made of various porphyrin and iron oxide compounds with different absorption spectra. If designed appropriately, these spectral modulators can effectively modify the incoming solar light spectrum by retarding photons in certain frequency ranges to suppress IR heating and thermalization so that PCE can be further increased under prolonged solar irradiation. The porphyrin compounds such as chlorophyllin and phthalocyanine, and their hybrids with iron oxides were synthesized to exhibit unique absorption spectra in the UV and IR regions.

As shown in Figure 1, the simulated solar light with typical spectrum passes the spectral modulator first. The TSM is a transparent film of 500 nm thick with average visible transmittance (AVT) of 85%. Upon passing TSM, the original simulated solar light is spectrally modulated in two different regions: retarding photons near UV to suppress thermalization, while heating can be reduced by removing the IR portion of the solar light

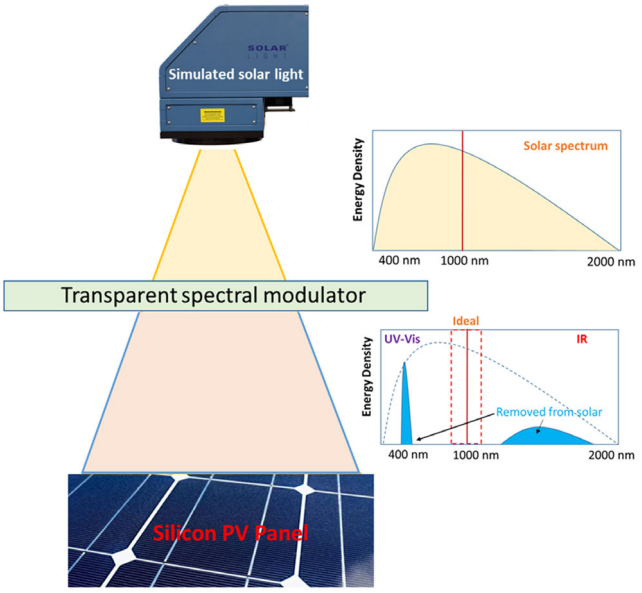

Figure 1. Schematic diagram showing the concept of modulated solar light for enhanced PCE.

(Figure 1). The porphyrin compounds typically exhibit a sharp peak near 400 nm and can absorb some high-energy photons (≈3.1 eV). Fe_3O_4@CuS is characterized with broad and strong IR absorption which can be used to suppress heating associated with sub-bandgap absorption.

2. Experimental Section

2.1. PV Measurement

An AOSHIKE Micro Solar panel with 54 mm × 54 mm dimensions was used as a standard in this study for PCE and output power (OPP) measurements. The measurement setup for *I–V* characterization is schematically shown in **Figure 2**. A solar simulator (Model number: LCS-100) was employed as a light source for a duration of 60 min for each experiment so that the heating effect was recorded. The solar panel surface temperature was monitored by using a thermal camera (FLIR, Inc.). The *I–V* curve measurement was performed by using Keithley 2400 SourceMeter (Figure 2). Figure 2 shows the experimental setup for measuring the *I–V* curves (Figure 2a) and a standard *I–V* curve (Figure 2b).

The efficiency of solar panels can be calculated using the following equation

$$\eta_{PV} = \frac{P_{max}}{P_{in}} = \frac{I_{SC} V_{OC} FF}{P_{in}} \quad (1)$$

where P_{max} is the maximum OPP, P_{in} is the input power (1.58 W), I_{SC} is the short-circuit current, V_{OC} is the open-circuit voltage, I_{MP} is the current at maximum power, V_{MP} is the voltage at maximum power, and FF is fill factor. The values of I_{SC}, V_{OC}, I_{max}, V_{max}, FF, P_{max}, and P_{in} are summarized in **Table 1**.

To maintain light power density on the PV panel surface, the TSM films are only partially covering the incoming solar light in the configuration shown in Figure 2c. As shown in this figure, portion of solar light is able to directly shine on the PV panel surface in the patterned region marked in yellow (Figure 2c) for enhanced I_{SC}, while the rest of the solar light is to be modulated by various thin films for reducing thermalization in the UV and heating in the IR regions in order to increase V_{OC}. The area ratio of TSM film-covered to the uncovered PV surface can be optimized for maximum PCE and OPP. It should be noted that the input power P_{in} was measured on the PV surface without any thin film shielding. A thermal camera was used to measure the PV surface temperature.

2.2. Materials Synthesis

The porphyrin compounds are naturally occurring and characterized with the porphyrin ring structures that are typically found in chlorophyll and hemoglobin.[23–28] The molecular structure of a porphyrin consists of a union of four pyrrole rings which are made from four carbons and one nitrogen. These pyrrole molecules are structurally connected to form a ring structure, known as porphyrin ring. Within the porphyrin ring, the tetradentate ligands for chelating metals are four nitrogen atoms holding the metal ions in the center. The central metal ions act as Lewis acids for accepting electron pairs from dianionic

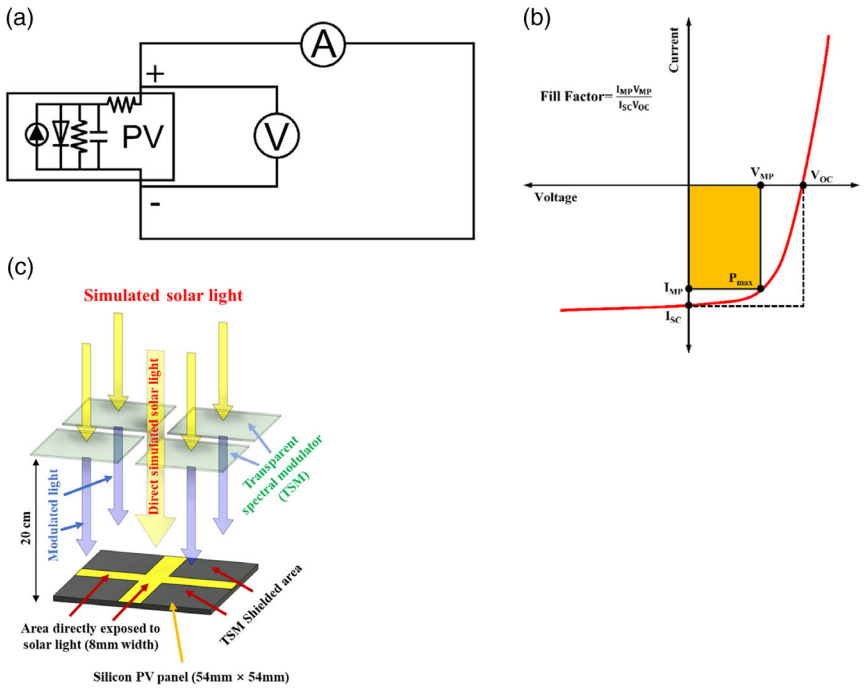

Figure 2. Schematic diagrams showing a) experimental setup of *I–V* measurement, b) the standard *I–V* curve with specified parameters, and c) configurations of solar light spectral modulation via transparent thin films over a commercial silicon PV panel.

Table 1. Values of I_{SC}, V_{OC}, I_{max}, V_{max}, FF, P_{max}, and P_{in} of silicon solar panel with different modulators at 60 min.

Modulator	I_{SC} [A]	V_{OC} [V]	I_{max} [A]	V_{max} [V]	FF	P_{max}	P_{in} [W]
Without TSM	0.192	1.94	0.156	1.59	0.666	0.248	1.58
Fe_3O_4@$Cu_{2-x}S$ 85% AVT	0.164	2.29	0.151	1.94	0.780	0.292	1.58
Chlorophyllin 85% AVT	0.167	2.27	0.161	1.84	0.781	0.296	1.58
Phthalocyanine	0.161	2.27	0.146	1.99	0.795	0.290	1.58
Chlorophyllin:Fe_3O_4@$Cu_{2-x}S$ 1:3 85% AVT	0.157	2.32	0.148	2.04	0.829	0.302	1.58
Chlorophyllin:phthalocyanine 1:3 85% AVT	0.151	2.27	0.154	2.02	0.904	0.310	1.58

porphyrin ligands. Due to the ring structure of the conjugated double bonds of porphyrins, porphyrins and their derivatives show unique absorption spectra, emission, charge transfer, and chelating properties.[24–28] The optical absorptions of porphyrins are typically characterized in the Soret (380–500 nm) and Q (500–800 nm) bands.[26] The unique optical behaviors of porphyrins have been applied in spectral selective solar harvesting and energy generation.[29–32] These compounds also utilize environmentally friendly green materials and processes.[28–33]

In this study, we synthesized porphyrin compounds of chlorophyllin, phthalocyanine, and their hybrid: chlorophyllin:phthalocyanine with 1:3 ratio. Hybrid between chlorophyllin and Fe_3O_4@$Cu_{2-X}S$ with 1:3 ratio (chlorophyllin:Fe_3O_4@$Cu_{2-X}S$) was also developed for spectral modulation. Chlorophyllin, phthalocyanine, chlorophyllin:phthalocyanine, and chlorophyllin:Fe_3O_4@$Cu_{2-X}S$ were dispersed in 10 wt% polyethylene glycol (PEG)/THF solution for thin film deposition.[33] The substrates used in this study were $2.54 \times 2.54\,cm^2$ microscope glass slides which were sonicated in acetone for 10 min, and then sonicated in IPA for another 10 min. Spin coating was employed to develop thin films with a spin coater (Laurell WS-400-6NPP\LITE). A 500 µL solution was dropped on the glass slide at the spinning speed of 3000 RPM. The film thickness and surface morphology were controlled by various spin coating parameters to control AVT.

Figure 3a shows the optical photographs of various solutions (from left to right): phthalocyanine ($3.57 \times 10^{-5}\,g\,cm^{-2}$), chlorophyllin:phthalocyanine (1:3, v:v) hybrid ($3.72 \times 10^{-5}\,g\,cm^{-2}$), chlorophyllin ($1.86 \times 10^{-5}\,g\,cm^{-2}$), chlorophyllin:$Fe_3O_4$@$Cu_{2-X}S$ (1:3, v:v) hybrid ($7.29 \times 10^{-5}\,g\,cm^{-2}$), and Fe_3O_4@$Cu_{2-X}S$ ($3.41 \times 10^{-5}\,g\,cm^{-2}$). The corresponding films of these solutions are shown in Figure 3b. As shown in Figure 3b, these films are quite transparent (AVT = 85%) due to their unique optical characteristics and 500 nm thickness.

Fe_3O_4 and Fe_3O_4@$Cu_{2-X}S$ nanoparticles were synthesized by following a previous report.[33] Both Fe_3O_4 and Fe_3O_4@ $Cu_{2-X}S$ nanoparticles were characterized by using transmission electron microscopy (TEM). **Figure 4** shows the TEM image of the Fe_3O_4 (Figure 4a) and Fe_3O_4@$Cu_{2-X}S$ (Figure 4b) nanoparticles. As

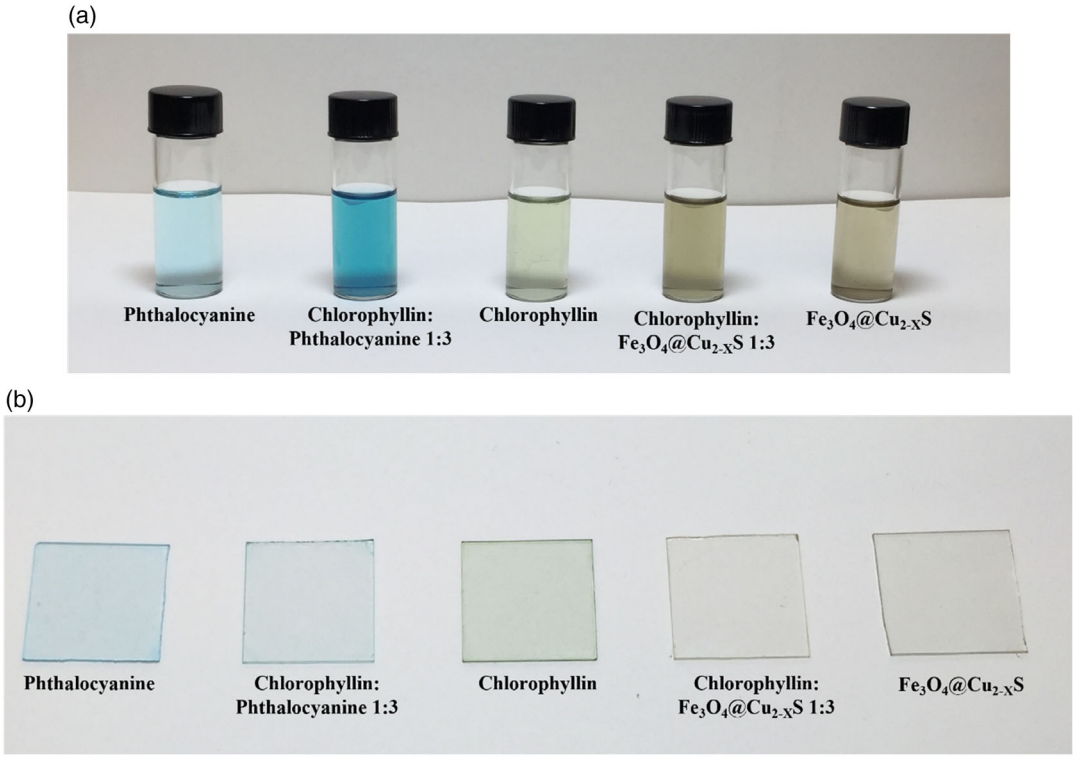

Figure 3. Photographs of a) solutions of (from left to right) phthalocyanine (3.57×10^{-5} g cm^{-2}), chlorophyllin:phthalocyanine (1:3, v:v) hybrid (3.72×10^{-5} g cm^{-2}), chlorophyllin (1.86×10^{-5} g cm^{-2}), chlorophyllin:$Fe_3O_4@Cu_{2-X}S$ (1:3, v:v) hybrid (7.29×10^{-5} g cm^{-2}), and $Fe_3O_4@Cu_{2-X}S$ (3.41×10^{-5} g cm^{-2}) and b) 25×25 mm^2 films of the solutions shown in (a).

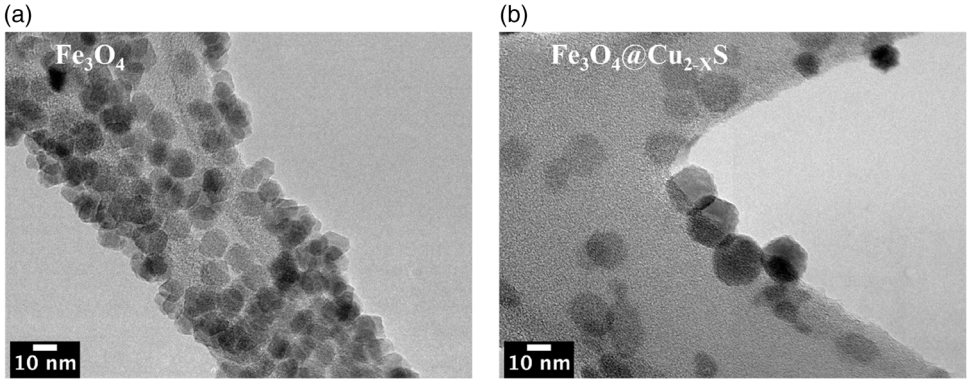

Figure 4. TEM images of a) Fe_3O_4 and b) $Fe_3O_4@Cu_{2-X}S$ nanoparticle.

shown in this figure, these nanoparticles are monodispersed with an average particle size of 10 nm for Fe_3O_4 and 15 nm for $Fe_3O_4@$ $Cu_{2-X}S$. The particle size of $Fe_3O_4@$ $Cu_{2-X}S$ is slightly larger due to the $Cu_{2-X}S$ coating on the Fe_3O_4 nanoparticles.[33]

3. Results

3.1. Optical Characterization

For developing the TSMs, the optical absorptions of these compounds and hybrids were characterized, including $Fe_3O_4@Cu_{2-X}S$, chlorophyllin, phthalocyanine, chlorophyllin: phthalocyanine, and chlorophyllin:$Fe_3O_4@Cu_{2-X}S$ hybrids for manipulation of the solar light spectrum. These compounds and hybrids exhibit unique absorption characteristics providing a versatile optical base for making spectral modulators in a wide range of photon frequency.

To observe their intrinsic optical behaviors, the absorption spectra were obtained from the solutions of these compounds and hybrids to avoid the bulk effects. **Figure 5** shows the absorption spectra of chlorophyllin, phthalocyanine, $Fe_3O_4@Cu_{2-X}S$, chlorophyllin:phthalocyanine (1:3, v/v), and chlorophyllin:$Fe_3O_4@Cu_{2-X}S$ (1:3, v/v) in THF. The

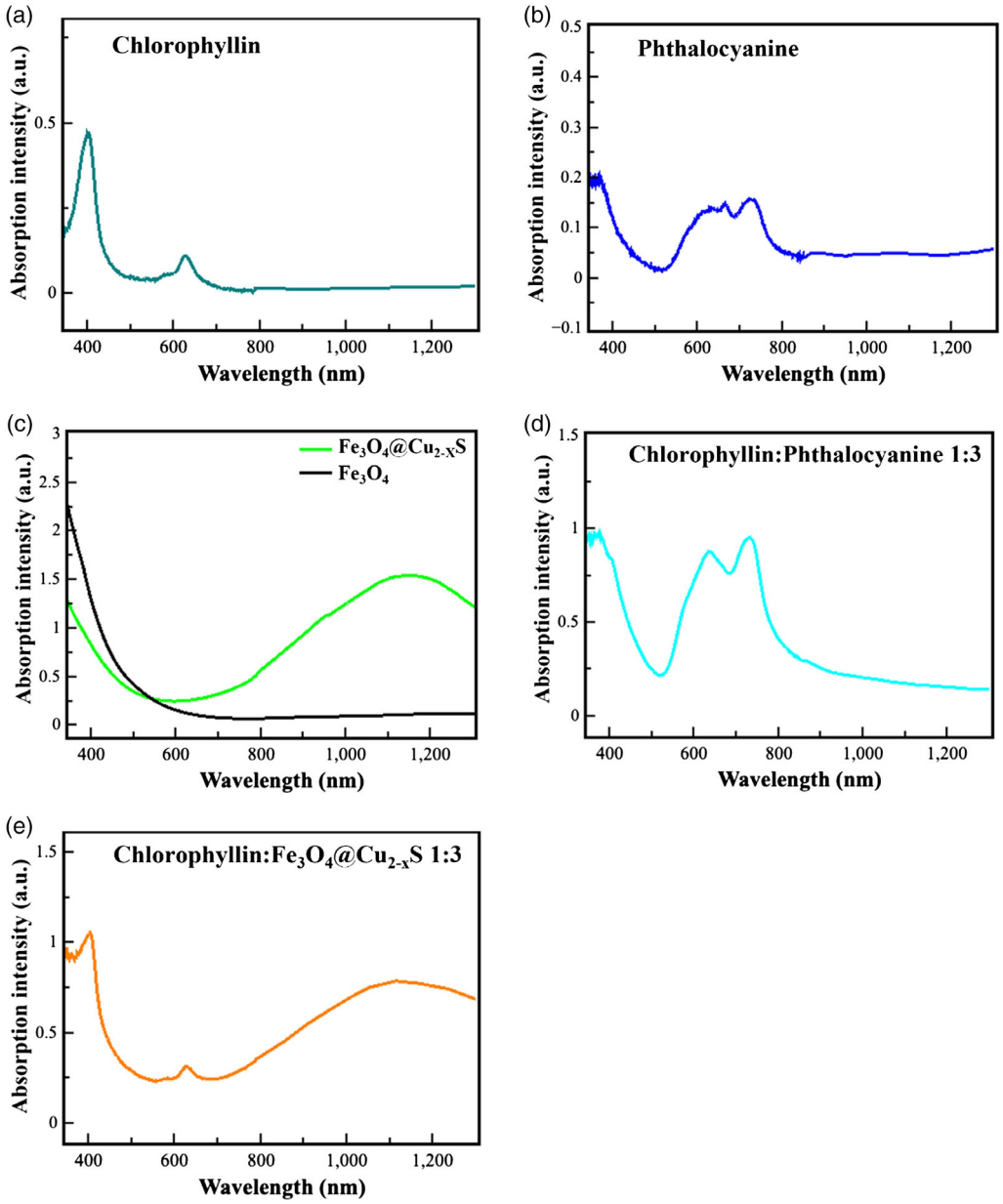

Figure 5. Absorption spectra of the porphyrins, iron oxides, and their hybrid solutions: a) chlorophyllin, b) phthalocyanine, c) Fe_3O_4 and $Fe_3O_4@Cu_{2-x}S$, d) chlorophyllin:phthalocyanine (1:3), and e) chlorophyllin:$Fe_3O_4@Cu_{2-x}S$ (1:3) in THF.

concentration is kept at 0.01 mg mL^{-1} for chlorophyllin, phthalocyanine, and $Fe_3O_4@Cu_{2-x}S$ in THF. The hybrid chlorophyllin:phthalocyanine contains 0.01 mg mL^{-1} of chlorophyllin and 0.03 mg mL^{-1} of phthalocyanine (1:3, v/v) and the hybrid chlorophyllin:$Fe_3O_4@Cu_{2-x}S$ contains 0.01 mg mL^{-1} of chlorophyllin and 0.03 mg mL^{-1} of $Fe_3O_4@Cu_{2-x}S$ (1:3, v/v).

As shown in Figure 5a, chlorophyllin has an intense absorption peak at 404 nm and a small one at 630 nm forming the so-called "saddle-like" spectrum. Phthalocyanine is characterized with a moderate peak at 370 nm, and a broad absorption between 550 nm and 750 nm (Figure 5b). These absorption characteristics are particularly useful for manipulating the solar spectrum especially in retarding the high-energy photons near 400 nm. Note that both chlorophyllin and phthalocyanine have low visible absorptions making their films quite transparent with high AVTs of 85% as shown in Figure 3a.

The $Fe_3O_4@Cu_{2-x}S$ nanoparticles are known for their IR absorptions.[33] Figure 5c shows the absorption spectra of both Fe_3O_4 and $Fe_3O_4@Cu_{2-x}S$ nanoparticles in solutions for comparison.[33] As shown in this figure, Fe_3O_4 typically exhibits a strong absorption in the UV region and rapidly subsides over the visible and IR regions. By coating a thin layer of $Cu_{2-x}S$ on the Fe_3O_4 nanoparticles, the $Fe_3O_4@Cu_{2-x}S$ solution exhibits a broad absorption peak extending beyond 1400 nm. This strong

IR absorption can be used to reduce the IR heating from the solar light. The IR absorption of $Fe_3O_4@Cu_{2-X}S$ has been attributed to the localized surface plasmonic resonance (LSPR) of $Cu_{2-X}S$ in the IR region.[33]

Figure 5d shows the absorption spectrum of chlorophyllin: phthalocyanine hybrid with 1:3 ratio. As shown in this figure, by adding a proportion of phthalocyanine in the chlorophyllin solution, the peak of chlorophyllin at 409 nm is shifted to 379 nm, while the 629 nm peak is not only broadened but also intensified with much stronger and double-peaked absorption between 629 and 723 nm. The overall spectrum is significantly modified with a more pronounced "U-shaped" spectrum as compared to those of pure chlorophyllin and phthalocyanine. The absorption spectrum of chlorophyllin:$Fe_3O_4@Cu_{2-X}S$ hybrid is shown in Figure 5e. As shown in this figure, there is a wide absorption with a maximum at 1132 nm while the UV peak has shifted to 409 nm. The hybrid has developed more pronounced absorption peaks in both UV and IR regions as compared to those of pure chlorophyllin and $Fe_3O_4@Cu_{2-X}S$. Interestingly, the absorption peak of chlorophyllin at 629 nm is merged in the spectrum of the chlorophyllin:$Fe_3O_4@Cu_{2-X}S$ hybrid. The spectrum shown in Figure 5e appears to combine the spectral features of both chlorophyllin and $Fe_3O_4@Cu_{2-X}S$: while UV absorption of the former is remained, the broad IR peak is also enhanced. These optical characteristics suggest the spectrally tunable nature of the hybrids in a wide range of frequency. These hybrid thin films can be used to spectrally modulate solar light in both amplitude and phase for matching of the photon energies with the bandgap of the silicon solar panel.

3.2. Silicon PV Panel Surface Temperature Profiles

Figure 6 shows the surface temperature profiles of the silicon solar panel with different TSMs. Note that the PV surface temperature is uniform as monitored by using the thermal camera As shown in Figure 6, the solar panel surface experiences significant temperature increase without TSM; the temperature rapidly increases to 92.9 from 22.9 °C only after 20 min. The light power is turned off at 60 min resulting in sharp fall of temperature.

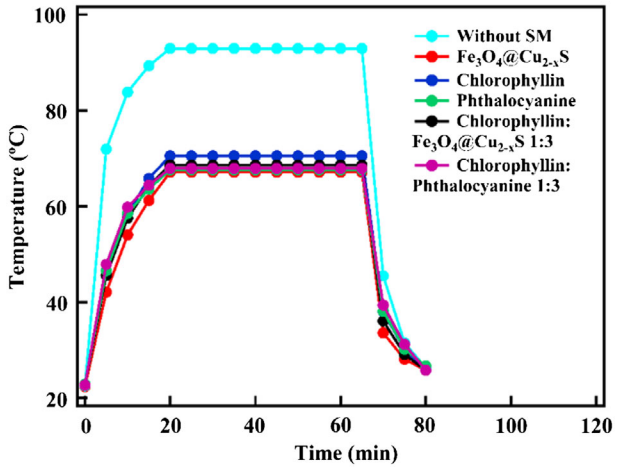

Figure 6. Temperature profiles of silicon solar panel with thin films of various compounds and hybrids as indicated.

However, with TSMs of different compounds and hybrids, the temperature increases are considerably reduced. All thin films of chlorophyllin, phthalocyanine, $Fe_3O_4@Cu_{2-X}S$, chlorophyllin:phthalocyanine, and chlorophyllin:$Fe_3O_4@Cu_{2-X}S$ lower temperature significantly by absorbing portion of the IR irradiation as shown in Figure 6. Consistently, the silicon solar panel surface temperatures are reduced to the range of 67.1–70.5 °C, about 24.1%–27.8% drop in temperature. As shown in this figure, $Fe_3O_4@Cu_{2-X}S$ thin film is the most effective in decreasing the PV surface temperature due to its strong IR absorption. It should be noted that these thin films (500 nm) are quite transparent with AVTs of 85% allowing majority of photons passing through them. As is well known, PCE is negatively dependent on the temperature increase with a temperature coefficient of −0.25% per °C.[34] As is expected, the temperature reduction by TSM will gain significant increase in PCE.

3.3. *I–V* Curves

Figure 7 shows the *I–V* curves of the silicon solar panel with different TSMs which are obtained at the 0 min (Figure 7a) and after 60 min solar irradiation (Figure 7b). As shown in Figure 7a, the V_{OC} values of the PV panels do not vary significantly with different TSMs due to insignificant heating at the beginning. However, I_{SC} values are all lowered slightly because the incoming light power is reduced by various TSMs. As shown in Figure 7b and Table 1, I_{SC} of the silicon panel at 60 min exhibits a normal value, 0.192 A. Expectedly as shown in Table 1, the I_{SC} values of those with different TSM films are all considerably reduced in the range of 0.15–0.17 A but only ≈3% decrease attributable to the light power loss through the TSM films, despite their high AVTs.

However, one can also see considerable increases in V_{OC} with different TSM films compared to that of the PV panel without TSM. As shown in Figure 7b, while V_{OC} is 1.94 V for the silicon PV panel without TSM, the V_{OC} values, respectively, increase to 2.29 V ($Fe_3O_4@Cu_{2-x}S$), 2.27 V (chlorophyllin), 2.27 V (phthalocyanine), 2.32 V (chlorophyllin:$Fe_3O_4@Cu_{2-x}S$), and 2.27 V (chlorophyllin:phthalocyanine). The time (temperature) dependences of V_{OC} are plotted in Figure 7c. As shown in this figure, the V_{OC} without TSM sharply decreases as a function of time (temperature) while all the V_{OC} values with TSMs are consistently higher and becoming less time (temperature) dependent (Table 1). Figure 7d shows the temperature dependences of V_{OC} with different TSMs. As shown in this figure, V_{OC} without TSM decreases linearly with temperature up to 92.9, while those with the TSMs remain at much less rates resulting in plateaus of V_{OC} versus time curves (Figure 7c).

The pronounced V_{OC} enhancement is attributable to the temperature reduction via IR absorption as evidenced in Figure 5, 6. The enhanced V_{OC} compensates for the I_{SC} loss associated with the reduced light power by TSM. Therefore, greater PCE is to be expected through improved FF. As shown in Table 1, the FF of the silicon solar panel with spectra modulators is, respectively, 0.780 ($Fe_3O_4@Cu_{2-x}S$), 0.781 (chlorophyllin), 0.795 (phthalocyanine), 0.829 (chlorophyllin:$Fe_3O_4@Cu_{2-x}S$), and 0.904 (chlorophyllin:phthalocyanine), all significantly higher than that without TSM (0.666). Among these thin films, the

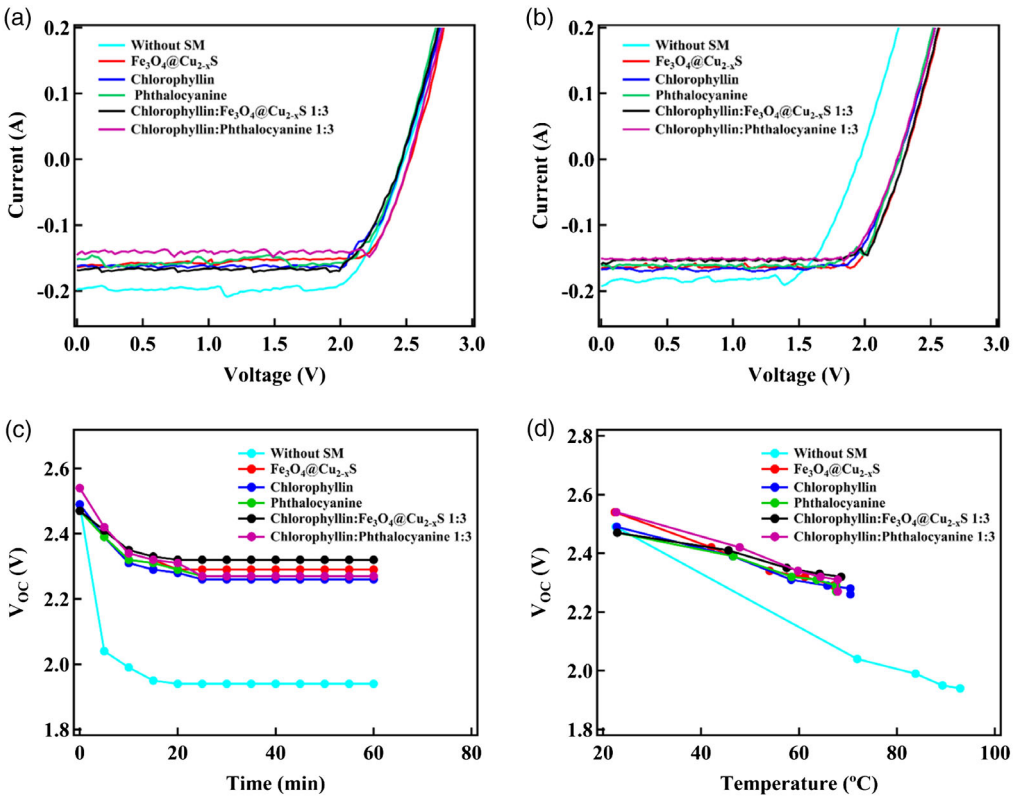

Figure 7. a) *I–V* curves of silicon solar panel with and without different spectral modulators at 0 min, b) *I–V* curves of silicon solar panel with and without different spectral modulators at 60 min, c) V_{OC} versus time for the silicon solar panel with and without different spectral modulators, and d) V_{OC} versus temperature for the silicon solar panel with and without different spectral modulators.

chlorophyllin:$Fe_3O_4@Cu_{2-x}S$ hybrid outperforms all others which are attributed to the unique optical absorptions as shown in Figure 5e. As shown in this figure, the hybrid exhibits a UV peak near 400 nm while exhibiting a broad range of IR absorption, combining the characteristics of both compounds.

3.4. Photon Conversion Efficiency

As shown in **Figure 8**, PCE of the silicon solar panel without TSM is 25.1% and it decreases to 16.3% after 60 min solar irradiation, resulting from the heating effect manifested by the negative temperature coefficient. However, as shown in Figure 8, the time dependences of PCE with various TSM films exhibit plateaus, indicating less temperature-dependent behaviors which are consistent to the data shown in Figure 6 that the PV panel surface temperatures are significantly reduced from above 92.9 °C to below 70.5 °C. Due to this surface temperature reduction, the maximum PCE by hybrid TSM of chlorophyllin: $Fe_3O_4@Cu_{2-X}S$ has reached 20.5% after 60 min solar irradiation, which is a 25.7% increase. We define PCE at 60 min the "long-term PCE" which is reasonable because it does not seem to change as a function of time (and temperature) after prolonged solar irradiation of 60 min. The long-term PCEs with other types of TSMs remain above 19.1% at 60 min. It is to be noted that the PCEs with TSMs are all lower than that without TSM at the beginning (i.e., no heating effect) due to reduced incoming light

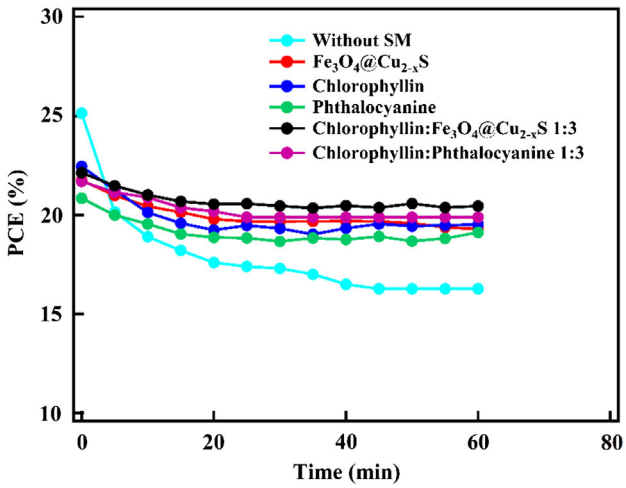

Figure 8. PCE versus time for the commercial silicon PV panel with and without different spectral modulators as indicated.

power. However, one can see greater PCEs at 0 min from chlorophyllin (22.4%), chlorophyllin:$Fe_3O_4@Cu_{2-X}S$ (21.7%), and chlorophyllin:phthalocyanine (21.7%) compared to that with TSMs of phthalocyanine (20.8%). These differences in PEC at 0 min can be attributable to the degree of thermalization associated with their absorptions in the UV regions. The PCE values of

those with different TSMs remain almost constant for prolonged solar irradiation up to 60 min. This unique TSM function provides important practical significance that the PV panels can retain considerable PCE under long-term solar irradiation and heating effect.

3.5. PV OPP

Quite similar behaviors were observed in the OPP as shown in **Figure 9**. Consistent with the PCEs (Figure 8), all OPPs of the silicon panel with TSMs exhibit much less time dependences up to 60 min in comparison to that without TSM. As shown in this figure, all OPPs remain above 0.290 W with the highest at 0.310 W for chlorophyllin:Fe_3O_4@$Cu_{2-X}S$. This is considerably higher than that without TSM, which is 0.247 W, a 25.5% increase. A common characteristic of OPP is that most of them are less time (temperature) dependent as compared to that without TSM. This behavior can be directly linked to the heating effect of the solar panel surface by solar irradiation. As shown in Figure 6, upon employing the spectral modulators, the solar panel surface temperatures are decreased effectively depending upon the optical absorptions of the compounds and hybrids. As all TSMs exhibit some NIR or IR absorptions, the heating effect is reduced, responsible for the less sensitive temperature dependences of the OPPs as compared to the silicon solar panel without any spectral modulators.

4. Discussion

The limitation of PCE, as explained by SQ model, mainly originates from thermalization, recombination, blackbody radiation, and sub-bandgap absorption. Considering recombination and blackbody radiation only taking small fractions in the losses, thermalization and sub-bandgap absorption are the main causes in limiting PCE. In this study, we consider the factors that influence PCE (and power) majorly from thermalization associated with photons near the UV region around 400 nm (≈3 eV) and sub-bandgap absorption above 1127 nm (1.1 eV) which contributes to IR heating under prolonged solar irradiation. If the high-energy photons can be partially absorbed by the spectral modulators, the thermalization effect can be reduced, leading to enhanced PCE under modulated solar light. On the other hand, removal of IR portion from the solar spectrum can significantly reduce PV surface temperature for maintaining PCE at an appreciable level for prolonged solar light irradiation.

The enhanced PCEs of silicon solar panel at 60 min by the spectral modulators are consistent with their optical absorptions as shown in Figure 5. Fe_3O_4@$Cu_{2-X}S$, due to LSPR, absorbs IR in a broad range beyond 1300 nm. For silicon, any solar light photons with wavelengths greater than 1127 nm (1.1 eV) do not contribute to the PV effect but generate thermal heating. The broad IR absorption by Fe_3O_4@$Cu_{2-X}S$ can therefore reduce solar surface heating as demonstrated in Figure 6. Therefore, to further reduce the temperature effect, the IR portion of the solar light should be effectively removed by TSM.

Among the PCEs with different TSMs at 0 min (i.e., no heating effect at the initial point of time), thermalization is the dominating factor which is associated with the photon energies near the UV region. The porphyrins and porphyrins:Fe_3O_4@$Cu_{2-X}S$ have absorption peaks at 404 nm which are at the high-energy boundary of the spectral response plot as shown in **Figure 10**. Spectral response (A/W) is defined as the ratio of the current generated by the solar panel to the power incident on the solar panel. As shown in Figure 10, the spectral response of a silicon solar panel is insignificant below 400 nm. It then increases with wavelength and approaches the ideal value near 1000 nm where the photo energy is close to the bandgap of silicon (1.12 eV), beyond which the response falls back to zero. As shown in Figure 5, both chlorophyllin and porphyrins:Fe_3O_4@$Cu_{2-X}S$ have strong peaks near 404 nm; considerable photons near 3.0 eV are absorbed, resulting in lowered thermalization. This removal of high-energy phones near 3.0 eV is partially responsible for enhanced PCEs at 0 min for both chlorophyllin and porphyrins:Fe_3O_4@$Cu_{2-X}S$ (Figure 8).

As shown in Figure 10, spectral response decreases sharply below 400 nm, and those photons with energies above 3.0 eV are not well utilized for generating electron–hole pairs.[19,20,35,36] Therefore, photons with energies near 4.1 eV (300 nm) have insignificant effects on thermalization. The UV peak of phthalocyanine is around 380 nm (3.2 eV) which is on the higher

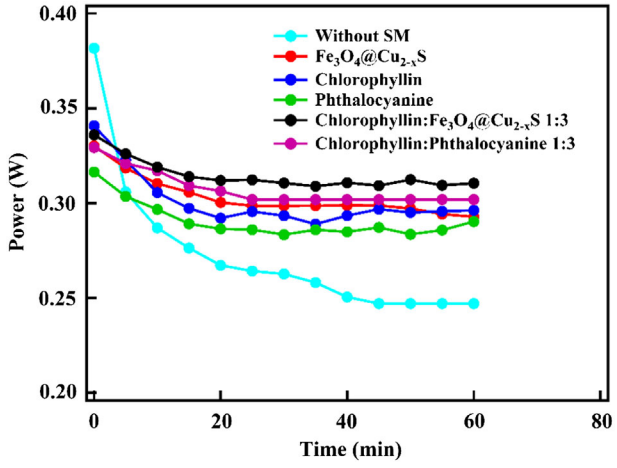

Figure 9. OPP versus time for the commercial silicon PV panel with and without different spectral modulators as indicated.

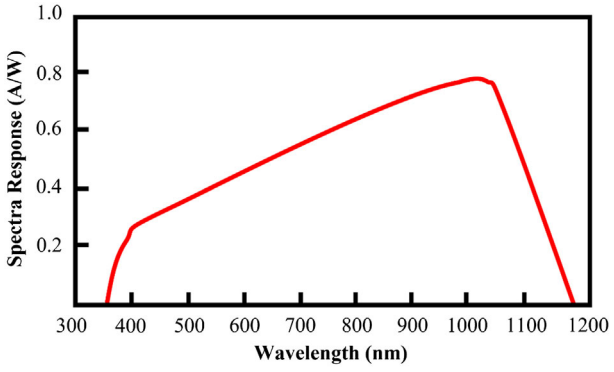

Figure 10. Schematic diagram showing the wavelength distribution of spectral response.

energy side of the spectral response curve. Compared to the chlorophyllin, it is less effective in suppressing of thermalization. Consequently, phthalocyanine has the lowest PCE at 0 min.

V_{OC}, the maximum voltage available from a solar panel, is characteristically dependent on temperature in association with dark saturation current I_o.[37,38] V_{OC} is logarithmically related to I_o: $V_{OC} = \ln (I_{SC}/I_o)$, where I_o is proportional to the intrinsic carrier concentration n_i, which is a thermally activated parameter given by the Boltzmann relationship: $n_i = \text{Exp}\ (-E/kT)$, where E is the bandgap linearly extrapolated to absolute zero, k is the Boltzmann constant, and T is the temperature. At elevated temperatures, V_{OC} will decrease due to increased I_o and n_i. On the other hand, the bandgap of a semiconductor decreases with increasing temperature due to reduction in bond energy. Smaller energy gap (E_g) will enable more electrons to overcome E_g, thus increasing n_i and I_o resulting in lowered V_{OC}.[39–45] The temperature profiles of the PV panel under various TSM films indicate consistent temperature reduction as shown in Figure 6. As a result of ≈25% temperature drop, V_{OC} gains a maximum of 19.8% increase compared to PV panels without TSMs, responsible for enhanced PCE and power through an improved FF up to 0.904 (Table 1).

There are two competing factors in maximizing PCE and power via patterned TSM over the PV panel. Enlarging the area with direct solar light exposure will increase I_{SC} but introduce various loss mechanisms such as thermalization and sub-bandgap absorption. However, increasing the TSM covered area will lower light power density, and hence decrease I_{SC}.[46–53] Therefore, this area ratio will have to be further optimized to achieve well-retained PCE and power for prolonged solar irradiation time. The high AVT values of TSM thin films are associated with their optical characteristics that all compounds and hybrids exhibit the saddle-like or U-shaped spectra with minimums in the visible region which allow for a wider frequency range of solar light to pass TSMs for generating electron–hole pairs. Furthermore, the TSM films are quite thin of 500 nm rendering them highly transparent (Figure 3).

The spectral modulation can also be photonically tuned to further reduce spectral losses. As shown in Figure 1, the photon energies near 400 nm all contribute to electron excitations to a broad range of energy states in the conduction band (i.e., the hot carriers). These excited electrons can interact with phonons for dissipation of their excess energy to the Si atoms as heat. However, chlorophyllin typically exhibits the "saddle-like" absorptions with a strong peak near 410 nm, and a small one at 630 nm, showing a valley in the visible region. These characteristics are ideal for solar light modulation because the peak at 410 nm can effectively remove photons with energies around 3.0 eV which is the short wavelength edge above which spectral response increases rather rapidly (Figure 10).[54] The photons near 1127 nm (1.1 eV) are ideally matched with the energy gap of silicon for enhanced PCE. The photons with energies smaller than 1.1 eV do not contribute to the photovoltaic effect but generate thermal heating. If effectively removed by spectral modulator, the PV panel temperature can be further lowered for increasing V_{OC}. Thus, removal of photons in the UV and the IR regions can effectively improve PCE. Juxtapositions of both determine the optimum solar spectral modulation for reaching even higher PCE especially for prolonged solar irradiation.

The optical absorptions of the porphyrin and iron oxides have been previously investigated.[28–33] The hybrids composed of these structurally different compounds exhibit unique characteristics with enhanced UV and IR absorptions which can be converted to thermal energy for more efficient solar light utilization.[55] Weinstein et al. reported a hybrid electric and thermal solar system for high solar-to-electricity efficiency at an operating temperature of 775 K.[56] This system relies on a quite complex design with a spectrally selective coating. The system is reportedly capable of converting solar energy to high-temperature thermal energy and subsequently to electricity via transparent aerogel layers. However, the light power may experience considerable attenuation after passing through the aerogel plate and reflected by light pipes before reaching the PV cell in this design. The design shown in Figure 2 addresses this problem by a patterned light path with light partly modulated to reduce heating and partly reaching the PV panel surface for retained light power.

Spectral splitting via hybrid photovoltaic thermal (PVT) has also been achieved with perovskite cells.[57,58] By integrating PV and PT, Wu et al. developed a hybrid PVT system via spectral selectively utilizing the near-infrared energy from the solar light.[57] They employed a photonic crystal of Si/GeO_2 to spectral selectively splitting the photon energy respectively for PV and PT in order to fully utilize the solar spectrum. The hybrid PVT design has achieved a solar-to-electrical efficiency of 29.3%. In this study, with a basic commercial silicon PV cell of low PCE, a simple hybrid coating results in appreciable PCE of 20.5% after 60 min solar irradiation. In practical terms, maintaining PCE at a steady level even after prolonged solar irradiation is highly significant.

5. Conclusions

The major goal of this study is to enhance PCE and OPP of silicon solar panel by spectrally modulating the incoming solar light via photonic thin films based on porphyrins and iron oxides taking advantages of their unique optical characteristics. By removal of photons in the UV and IR regions, the major spectral losses are reduced including thermalization of hot carriers and thermal heating of IR radiation. As a result, the PCE of the commercial silicon PV panel has reached the highest of 20.5% with TSMs at 60 min, which is significantly higher than that of the original silicon panel (16.3% at 60 min). The enhanced PCE for prolonged solar irradiation time will have important practical significance for solar energy applications. The spectral modulation approach is technically straightforward, economically viable, and requiring no complicated processes in developing new materials and device architecture. For instance, a spectral modulator above the solar panel with partial shield can reduce the surface temperature effectively while maintaining the level of I_{SC}. Proportional removal of some high-energy photons near the UV edge can suppress thermalization and reduction of thermal heating can be achieved by filtering the IR radiation from the solar light. This solar spectral modulation strategy will show promise in practical applications of solar panels with much improved efficiency.

Acknowledgements

The authors acknowledge the financial support from National Science Foundation CMMI-1635089 and CMMI-1953009.

Conflict of Interest

The authors declare no conflict of interest.

Data Availability Statement

The data that support the findings of this study are available on request from the corresponding author. The data are not publicly available due to privacy or ethical restrictions.

Keywords

hot carriers, photon conversion efficiency, porphyrin hybrids, solar harvesting, spectral modulation, sub-bandgap absorption, thermalization

Received: February 14, 2023
Revised: March 14, 2023
Published online:

[1] B. Parida, S. Iniyan, R. Goic, *Renewable Sustainable Energy Rev.* **2011**, *15*, 1625.
[2] D. Poponi, *Sol. Energy* **2003**, *74*, 331.
[3] M. Mehrtash, Q. Guillermo, D. Yvan, R. Daniel, in *Proc. of the 20th Annual Int. Conf. on Mechanical Engineering-ITSME2012*, Shiraz, Iran **2012**, pp. 16–18.
[4] J. D. Mondol, Y. G. Yohanis, B. Norton, *Renewable Energy* **2007**, *32*, 118.
[5] M. M. Fouad, L. A. Shihata, E. I. Morgan, *Renewable Sustainable Energy Rev.* **2017**, *80*, 1499.
[6] M. Ito, K. Kato, H. Sugihara, T. Kichimi, J. Kichimi, K. Kurokawa, *Sol. Energy Mater. Sol. Cells* **2003**, *75*, 507.
[7] X. Zhou, J. Yang, F. Wang, B. Xiao, *Renewable Sustainable Energy Rev.* **2009**, *13*, 736.
[8] E. Cunow, B. Giesler, *Sol. Energy Mater. Sol. Cells* **2001**, *67*, 459.
[9] P. Irace, H. Brandon, Mechanical Engineering and Materials Science Independent Study, **2017**, p. 50.
[10] T. M. Razykov, C. S. Ferekides, D. Morel, E. Stefanakos, H. S. Ullal, H. M. Upadhyaya, *Sol. Energy* **2011**, *85*, 1580.
[11] International Energy Agency, Technology Roadmap-Solar Photovoltaic Energy, http://www.iea-pvps.org, (accessed: October 2022).
[12] EPIA Report, The Solar Photovoltaic Electricity Empowering the World, http://www.greenpeace.org/international/en/publications/reports/Solar-Generation-6/, (accessed: October 2022).
[13] A. Jäger-Waldau, M. Szabó, F. Monforti-Ferrario, H. Bloem, T. Huld, R. L. Arantegui, Renewable Energy Snapshots, **2011**, http://www.jrc.ec.europa.eu/, (accessed: October 2022).
[14] M. Yamaguchi, H. Yamada, Y. Katsumata, K. Lee, K. Araki, N. Kojima, *J. Mater. Res.* **2017**, *32*, 3445.
[15] K. Masuko, M. Shigematsu, T. Hashiguchi, D. Fujishima, M. Kai, N. Yoshimura, T. Yamaguchi, Y. Ichihashi, T. Mishima, N. Matsubara, T. Yamanishi, *IEEE J. Photovoltaics* **2014**, *4*, 1433.
[16] T. D. Lee, A. U. Ebong, *Renewable Sustainable Energy Rev.* **2017**, *70*, 1286.
[17] R. Wang, M. Mujahid, Y. Duan, Z. Wang, J. Xue, Y. Yang, *Adv. Funct. Mater.* **2019**, *29*, 1808843.
[18] W. Shockley, H. J. Queisser, *J. Appl. Phys.* **1961**, *32*, 510.
[19] Y. Lee, C. Park, N. Balaji, Y. J. Lee, V. A. Dao, *Isr. J. Chem.* **2015**, *55*, 1050.
[20] Y. Zhang, X. Jia, S. Liu, B. Zhang, K. Lin, J. Zhang, G. Conibeer, *Sol. Energy Mater. Sol. Cells* **2021**, *225*, 111073.
[21] A. Le Bris, J. Rodiere, C. Colin, S. Collin, J. L. Pelouard, R. Esteban, M. Laroche, J. J. Greffet, J. F. Guillemoles, *IEEE J. Photovoltaics* **2012**, *2*, 506.
[22] C. Strümpel, M. McCann, G. Beaucarne, V. Arkhipov, A. Slaoui, V. Švrček, C. del Cañizo, I. Tobias, *Sol. Energy Mater. Sol. Cells* **2007**, *91*, 238.
[23] G. Layer, D. Jahn, E. Deery, A. D. Lawrence, M. J. Warren, in *Comprehensive Natural Products II*, Elsevier, Amsterdam **2010**, pp. 445–499.
[24] D. Sarkar, A. Sharma, G. Talukder, *Mutat. Res.* **1994**, *318*, 239.
[25] M. Gouterman, *J. Mol. Spectrosc.* **1961**, *6*, 138.
[26] P. A. Lewis, in *The Gardner Sward Handbook: Paint and Coating Testing Manual*, ASTM International, Philadelphia, PA, USA **1995**, p. 190.
[27] H. Yin, S. Chen, S. H. Cheung, H. W. Li, Y. Xie, S. W. Tsang, X. Zhu, S. K. So, *J. Mater. Chem. C* **2018**, *6*, 9111.
[28] M. Lyu, J. Lin, J. Krupczak, D. Shi, *Adv. Sustainable Syst.* **2021**, *5*, 2100006.
[29] Y. Zhao, A. Dunn, D. Shi, *MRS Commun.* **2019**, *9*, 675.
[30] Y. Zhao, J. Lin, D. M. Kundrat, M. Bonmarin, J. Krupczak, S. V. Thomas, M. Lyu, D. Shi, *J. Phys. Chem. C* **2020**, *124*, 1575.
[31] J. Lin, D. Shi, *Appl. Phys. Rev.* **2021**, *8*, 011302.
[32] J. Lin, Y. Wang, M. Lyu, Z. Deng, D. Shi, *Sol. Energy Mater. Sol. Cells* **2022**, *243*, 111788.
[33] J. Lin, Y. Zhao, D. Shi, *MRS Commun.* **2020**, *10*, 155.
[34] B. R. Paudyal, A. G. Imenes, *Sol. Energy* **2021**, *224*, 425.
[35] B. Ehrler, E. Alarcón-Lladó, S. W. Tabernig, T. Veeken, E. C. Garnett, A. Polman, *ACS Energy Lett.* **2020**, *5*, 3029.
[36] Z. Omair, G. Scranton, L. M. Pazos-Outón, T. P. Xiao, M. A. Steiner, V. Ganapati, P. F. Peterson, J. Holzrichter, H. Atwater, E. Yablonovitch, *PNAS* **2019**, *116*, 15356.
[37] A. B. Sproul, M. A. Green, *J. Appl. Phys.* **1991**, *70*, 846.
[38] S. Yoon, V. Garboushian. in *Proc. of 1994 IEEE 1st World Conf. on Photovoltaic Energy Conversion-WCPEC (A Joint Conf. of PVSC, PVSEC and PSEC)*, Waikoloa, HI, USA **1994**, *2*, pp. 1500–1504.
[39] R. V. Singh, C. M. Singal, *Sol. Cells* **1983**, *10*, 155.
[40] N. Barth, R. Jovanovic, S. Ahzi, M. A. Khaleel, *Sol. Energy Mater. Sol. Cells* **2016**, *148*, 87.
[41] J. C. Fan, *Sol. Cells* **1986**, *17*, 309.
[42] K. Emery, J. Burdick, Y. Caiyem, D. Dunlavy, H. Field, B. Kroposki, T. Moriarty, L. Ottoson, S. Rummel, T. Strand, M. W. Wanlass, in *Conf. Record of the Twenty Fifth IEEE Photovoltaic Specialists Conf.-1996*, Washington, DC, USA **1996**, pp. 1275–1278.
[43] H. Steinkemper, I. Geisemeyer, M. C. Schubert, W. Warta, S. W. Glunz, *IEEE J. Photovoltaics* **2017**, *7*, 450–457.
[44] C. P. Thompson, S. Hegedus, W. Shafarman, D. Desai, in *2008 33rd IEEE Photovoltaic Specialists Conf.*, IEEE, Piscataway, NJ **2008**, pp. 1–6.
[45] E. A. Katz, D. Faiman, S. M. Tuladhar, J. M. Kroon, M. M. Wienk, T. Fromherz, F. Padinger, C. J. Brabec, N. S. Sariciftci, *J. Appl. Phys.* **2001**, *90*, 5343.
[46] Effect of Temperature, https://www.pveducation.org/pvcdrom/solar-panel-operation/effect-of-temperature#:≈:text=However%2C%20this%20is%20a%20TSMall, than%20the%20semiconductor%20material%20properties (accessed: October 2022).
[47] S. H. Liu, E. J. Simburger, J. Matsumoto, A. Garcia III, J. Ross, J. Nocerino, *Prog. Photovoltaics Res. Appl.* **2005**, *13*, 149.

[48] S. Dubey, J. N. Sarvaiya, B. Seshadri, *Energy Procedia* **2013**, *33*, 311.
[49] N. H. Zaini, M. Z. Ab Kadir, M. Izadi, N. I. Ahmad, M. A. Radzi, N. Azis, in *2015 IEEE Conf. on Energy Conversion (CENCON)*, IEEE, Piscataway, NJ **2015**, pp. 249–253.
[50] M. Taguchi, E. Maruyama, M. Tanaka, *Jpn. J. Appl. Phys.* **2008**, *47*, 814.
[51] A. V. Sachenko, Y. V. Kryuchenko, V. P. Kostylyov, R. M. Korkishko, I. O. Sokolovskyi, A. S. Abramov, S. N. Abolmasov, D. A. Andronikov, A. V. Bobyl, I. E. Panaiotti, E. I. Terukov, *Tech. Phys. Lett.* **2016**, *42*, 313.
[52] S. K. Krawczyk, A. Jakubowski, M. Żurawska, *Solar Cells* **1981**, *4*, 187.
[53] K. Nishioka, T. Sueto, M. Uchida, Y. Ota, *J. Electron. Mater.* **2010**, *39*, 704.
[54] A. M. G. Amillo, T. Huld, P. Vourlioti, R. Müller, M. Norton, *Energies* **2015**, *8*, 3455.
[55] J. Lin, J. Krupczak, D. Shi, *MRS Commun.* **2022**, *12*, 1225.
[56] L. A. Weinstein, K. McEnaney, E. Strobach, S. Yang, B. Bhatia, L. Zhao, Y. Huang, J. Loomis, F. Cao, S. V. Boriskina, Z. Ren, E. N. Wang, G. Chen, *Joule* **2018**, *2*, 962.
[57] Z. Wu, J. Wang, S. Hou, L. Yin, Y. Qiao, Z. Tang, S. Zhang, J. Mao, X. Liu, Q. Zhang, F. Cao, *Sol. RRL* **2023**, *7*, 2201072.
[58] Z. Wu, J. Wang, L. Yin, J. Mao, X. Liu, Q. Zhang, F. Cao, *Sol. RRL* **2022**, *6*, 2200283.